Rheological signature of microswimmer phase-locking under flow

Mohd Suhail Rizvi [1,*] Abdessamad Nait-Ouhra,[1,2] Alexander Farutin,[1]
Philippe Peyla,[1] Salima Rafai,[1] and Chaouqi Misbah[1,†]

[1]*Laboratoire Interdisciplinaire de Physique, Université Grenoble Alpes and CNRS, F-38000 Grenoble, France*
[2]*LaMCScI, Faculty of Sciences, Mohammed V University of Rabat, 1014, Rabat, Morocco*

Understanding macroscopic behaviors of suspensions of active particles is a challenging issue in the study of living fluids. We investigate the response of shape-change driven microswimmers to an external flow. In particular, we calculate the viscosity of the dilute suspension of active microswimmers when the flow timescale is close to that of the swimmer activity, resulting in an ample contribution of the swimmer activity to rheology. We find that the shape activity leads to either an increase or a decrease of the effective viscosity, depending on the shear rate. These opposite behaviors occurring for the same microswimmer originate from a phase-locking phenomenon between the swimmer shape oscillations and the applied flow. A simplified analytical model remarkably reproduces the results of full simulations, and offers a promising framework for the derivation of macroscopic constitutive laws for active matter.

I. INTRODUCTION

Because of the wide variety of environments and ecosystems where microorganisms live, their evolution has resulted in various ways of moving (gliding, twitching, swimming) towards their favorite chemical or food sources [1,2]. Examples of propulsion machinery include the cyclic beating of two flagella in a breast-stroke manner by *Chlamydomonas reinhardtii* [2], rotation of a helical flagellar bundle by *Escherichia coli* [1], or the repeated body deformation of the *Eutreptiella gymnastica* [3]. Similarly, cells of the immune system develop ample shape changes to fight pathogens in complex environments, such as the extracellular matrix within tissues. There is now increasing evidence that cells of the immune system, among others, are able to swim in a fluid [4,5]. The micron size of cells and their low velocity ensure that inertia is negligible. Despite the diversity of microorganisms, they all share a common feature, namely, the repetitive and nonreciprocal temporal variation of forces on the fluid.

A popular swimmer model is the constant force dipole which often discards the details of the active force generation machinery and retains the average behavior over one cycle of time-dependent active forces [6,7]. This swimmer can be categorized into two types: "puller" (e.g., *C. reinhardtii* [7,8]) and "pusher" (e.g., *E. coli* [9]), depending on the sign of the dipole. A suspension of microswimmers displays unusual macroscopic rheology [8,10–14]: a pushers' (pullers') suspension exhibits a lower (higher) effective viscosity than their respective passive counterparts. Furthermore, experimental studies have also shown a rich rheological behavior rarely recovered in theoretical models. For instance, a shear-thinning [8] (shear-thickening [13,14]) nature of the pullers' (pushers')

---

*mohd-suhail.rizvi@univ-grenoble-alpes.fr
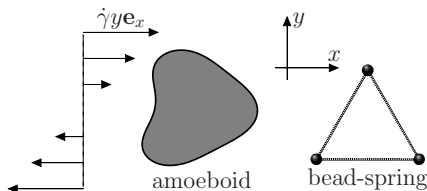†chaouqi.misbah@univ-grenoble-alpes.fr

FIG. 1. Schematics of bead-spring and amoeboid microswimmers in shear flow.

suspensions has been reported. So far, the main key ingredient of the models explaining the rheology of microswimmers (increase and decrease of viscosity due to activity), is rotational diffusion [15]. However, in general, microswimmers exhibit shape deformations (flagella motion, body shape changes, etc.) and their impact needs to be explored. It has been shown recently that the cyclic motion of flagella makes the cell follow very specific Jeffery orbits that can affect rheology [16].

In order to decipher the rheological behavior of swimmer suspensions, it seems relevant to consider the coupling between the flow and the time-dependent active forces. More generally, in most cases, shape changes of microswimmers are intrinsically related to propulsion mechanisms (flagellar beating or shape deformations). We show that shape change activity not only contributes to the viscosity of the suspension without evoking noise, but also uncovers new subtle effects. In particular, the active contribution to the viscosity is found to switch between positive and negative values depending on the magnitude of the applied shear flow for a given type (puller or pusher) of microswimmer. This results from a nonlinear coupling between the swimmer and the applied flow.

A widely adopted model for swimmers consists of a thin rodlike rigid shape with a given stresslet (force dipole), which is aligned with the rod and is either inward (puller) or outward (pusher). A deterministic rod under linear shear flow is known to exhibit tumbling (Jeffery orbit) and spends the same time in the upper and lower halves of the shear plane. As a consequence, no resulting active contribution to the viscosity is expected on average. Noise breaks this symmetry (the rod then spends more time in the upper half plane), giving rise to a net contribution of the active stress to the rheology [6,12]. Hence, in all available models, noise (due, for instance, to rotational diffusivity or tumbling of the microswimmers) is a crucial ingredient to recover a net effect of average active stresses on viscosity. Real swimmers undergo repeated shape changes, which lead to a nontrivial contribution to the active stress. Here we will address the effect of shape activity on the rheology of microswimmer suspensions in two cases: amoeboid swimmer and bead-spring microswimmer.

II. RHEOLOGY OF MICROSWIMMER SUSPENSIONS

A. Amoeboid microswimmer

We begin our study by considering an amoeboid microswimmer in two-dimensional space (Fig. 1) characterized by a fluid-filled impermeable membrane of perimeter P_0 and enclosed area A_0 immersed in another fluid [17,18]. The swimmer has reduced area $\Gamma = 4\pi A_0/P_0^2$ (measuring deviation from a circle for which $\Gamma = 1$), which allows the microswimmer deformation.

η and $\lambda\eta$ denote the respective viscosities of external and internal fluids, where λ is the viscosity contrast. We consider the flow in and outside of the swimmer to be in the Stokes regime, obeying

$$\nabla \cdot \mathbf{u} = 0, \quad \eta_i \nabla^2 \mathbf{u}(\mathbf{r}, t) = \nabla P(\mathbf{r}, t), \tag{1}$$

where $\mathbf{u}$ and P are the fluid velocity and pressure, respectively, and $\eta_i = \eta$ or $\lambda\eta$ outside and inside the swimmer, respectively. The shape of the swimmer at time t is described by a closed curve $\mathbf{X}(s, t)$ in the x-y plane, where s is the curvilinear coordinate along the membrane. We represent the membrane position $\mathbf{X}$ by a Fourier series

$$\mathbf{X}(s) = \sum_{k=-k_{\max}}^{k_{\max}} \mathbf{X}_k \exp{(2\pi i k s)} \tag{2}$$

with complex amplitudes $\mathbf{X}_k$. Given the inextensibility of the membrane, the application of active force results in the generation of tension $\xi(s, t)$. The resultant passive force density on the swimmer surface is, therefore, given by

$$\mathbf{f}(s, t) = -\xi(s, t)c(s, t)\mathbf{n}(s, t) + \frac{d\xi(s, t)}{ds}\mathbf{t}(s, t), \tag{3}$$

where $\mathbf{n}$ and $\mathbf{t}$ are the normal and tangential unit vectors to the membrane surface, respectively. In addition to the passive membrane forces, we have to specify the active forces. For simplicity, these are taken to be normal (i.e., $F_a\mathbf{n}$) to the membrane and are decomposed in Fourier harmonics as

$$F_a(s, t) = \sum_{n=-n_{\max}, n \neq -1, 0, 1}^{n=n_{\max}} f_n(t)e^{ins}. \tag{4}$$

In the above, due to the fluid incompressibility the term corresponding to $n = 0$, which corresponds to a constant pressure jump across the membrane, plays no role. For simplicity we set $f_{\pm 1}(t) = 0$ (we have kept the model as simple as possible by considering only the second and third harmonics). We require at least two harmonics to induce shape deformations which are not invariant under time reversal, a necessary condition for autonomous swimming (Scallop theorem [19]). We set $f_2 = -f_a \cos(\omega_a t)/2$ and $f_3 = f_a \sin(\omega_a t)/2$, where ω_a is the stroke frequency and f_a is the active force amplitude. By considering only the real part of the Fourier harmonics expansion, we get the following active force:

$$F_a(s, t) = -f_a \cos(\omega_a t) \cos(2s) + f_a \sin(\omega_a t) \cos(3s). \tag{5}$$

Including higher harmonics is not decisive for the swimming phenomenon [20]. Therefore, the total force density on the swimmer surface is given by

$$\mathbf{F}(s, t) = F_a(s, t)\mathbf{n} + \mathbf{f}(s, t) + \mathbf{f}_o(t) + f_t(t)\mathbf{t}(s, t), \tag{6}$$

where $\mathbf{f}_o(t)$ and $f_t(t)\mathbf{t}(s, t)$ allows one to fulfill the force-free and torque-free conditions on the swimmer surface [18].

We define the nondimensional active force amplitude $f = f_a/(\eta\omega_a)$ as the ratio between the timescales of the swimming strokes and fluid flow. This, together with hydrodynamic interactions, results in autonomous propulsion along a straight line [17,20,21]. We make use of Green's function techniques to write the membrane velocity as an integral equation expressing nonlocal hydrodynamics effects [22]. Details of the boundary integral method based numerical technique are given in Appendix A.

The system is subjected to a linear shear flow of strength $\dot{\gamma}$ (Fig. 1) and the effective viscosity $\eta_{\text{eff}} = \langle \sigma_{xy} \rangle / \dot{\gamma}$ is measured as the ratio of average shear stress (active+passive) and applied shear rate. For a suspension with swimmer volume fraction ϕ, the intrinsic viscosity of the suspension $[\eta] = (\eta_{\text{eff}} - \eta)/\phi\eta$ is obtained by Batchelor's formula [23] as

$$[\eta] = \frac{1}{A_0 \dot{\gamma} \eta} \left\langle -\int F_x y \, ds + \eta(\lambda - 1)\int (u_x n_y + u_y n_x) ds \right\rangle, \tag{7}$$

where the x and y subscripts denote the x and y components, respectively, and $\mathbf{u}$ is the membrane velocity. Here the integral is performed over the membrane and $\langle \cdot \rangle$ refers to the time average (to be specified later). We define the contribution of activity to viscosity as $\Delta\eta = [\eta] - [\eta]_p$, where $[\eta]_p$ is the intrinsic viscosity of the passive suspension, obtained by setting the active force to zero.

The dependence of intrinsic viscosity on the applied shear rates is summarized in Fig. 2. We observe that the contribution of activity switches from positive to negative at some critical shear rate $\dot{\gamma}_c$. Three successive regimes of $[\eta]$ are observed. For low values of shear rates ($\dot{\gamma} < \dot{\gamma}_-$), $d[\eta]/d\dot{\gamma} > 0$ followed by $d[\eta]/d\dot{\gamma} < 0$ for intermediate values of shear rates. Finally, for high shear rates ($\dot{\gamma} > \dot{\gamma}_+$), $[\eta]$ again starts to increase with $\dot{\gamma}$. The transitions occur at shear rates $\dot{\gamma}_{\mp}$ which depend on the active force amplitude. A remarkable observation is that the normalized transition
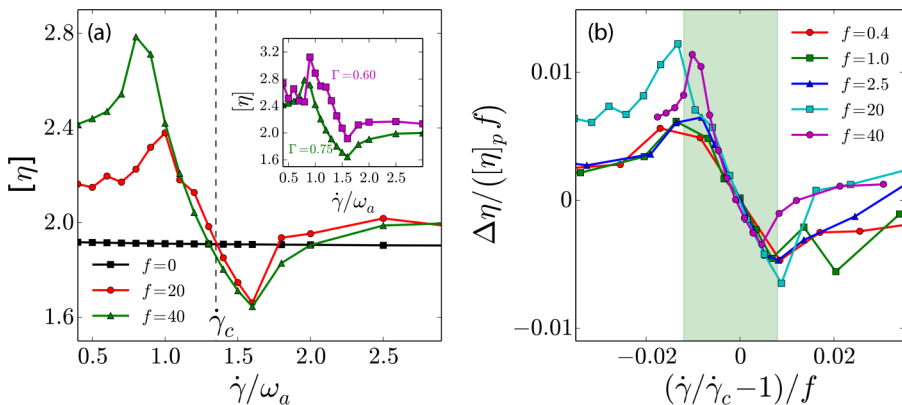
FIG. 2. (a) Intrinsic viscosities of passive vesicles ($f = 0$) and amoeboid microswimmers ($f > 0$) for $\Gamma = 0.75$. $\dot{\gamma}_c$ marks the shear rate at which $\Delta\eta = 0$. Inset shows $[\eta]$ for different Γ with $f = 40$. (b) For small f, the normalization of the shear rate difference $\dot{\gamma}/\dot{\gamma}_c - 1$ and the active contribution to viscosity $\Delta\eta/[\eta]_p$ by f results in a reasonable collapse of the curves, especially in the central region; $\lambda = 20$.

shear rates $(\dot{\gamma}_{\mp}/\dot{\gamma}_c - 1)/f$ do not depend on the active force amplitudes f [Fig. 2(b)] (see Sec. III A for the motivation for this scaling).

In two dimensions a dilute passive suspension of disks provides $[\eta]_p = 2$ [equal to 5/2 for spheres in three dimensions (3D)] [24,25]. For vesicles, it is about 1.8 for $\Gamma = 0.75$ [Fig. 2(a), black]. In the presence of activity, the intrinsic viscosity attains values close to 3 [Fig. 2(a), green], showing the importance of activity (in the same proportion as found experimentally in 3D for *Chlamydomonas* [8]). From the data shown in Fig. 2(a) (inset) obtained for two different deflation parameters Γ, we expect this value to be significantly larger than 3 for more deflated shapes such as that of *Eutreptiella gymnastica*. An estimate of active forces generated by the cells shows that the dimensionless force $f \gg 1$ (assuming $\eta \approx 1$ cP and $\omega_a \approx 1$ s^{-1}) [26]. Owing to the membrane incompressibility $[\eta]$ saturates beyond a value of f of a few tens for $\Gamma = 0.75$ [Fig. 2(b)]. In order to gain insights into this rheological behavior, we estimated the effective viscosity of the dilute suspension of a much simpler system of active swimmer composed of beads and springs.

B. Bead-spring microswimmer

We consider a bead-spring microswimmer where three identical beads (radius a each) are connected by linear springs (length $l \gg a$, stiffness $k = $ force/strain) in a triangular manner (Fig. 1) [27]. This is a variant of the model of flagellar swimming of *C. reinhardtii* proposed in [28,29]. In the Stokes regime, that is, Re $= 0$, we can write the equations of motion for each bead as

$$\frac{d\mathbf{r}_i}{dt} = \mu\mathbf{f}_i(\mathbf{r}, t) + \sum_{j \neq i} \mathcal{G}_{ij} \cdot \mathbf{f}_j(\mathbf{r}, t) + \mathbf{u}^\infty, \tag{8}$$

where $\mu = (6\pi\eta a)^{-1}$ is the bead mobility, $\mathbf{u}^\infty$ is the externally imposed flow, and $\mathcal{G}_{ij}$ is the Oseen tensor

$$\mathcal{G}_{ij}(\mathbf{r}_{ij}) = \frac{1}{8\pi\eta}\left(\frac{\mathbf{I}}{r_{ij}} + \frac{\mathbf{r}_{ij} \otimes \mathbf{r}_{ij}}{r_{ij}^3}\right) \tag{9}$$

describing the hydrodynamic interaction between the ith and jth beads, and $\mathbf{f}_i$ is the total force acting on the ith bead.

By virtue of the hydrodynamic interactions among the beads, the active forces $f_{ij} = f_a \sin(\omega_a t + \alpha_{ij})$ between the ith and jth beads along the connecting spring lead to autonomous translation
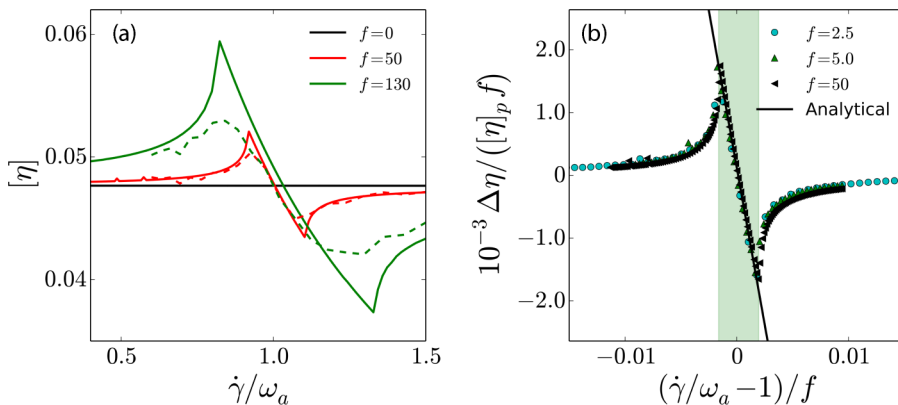
FIG. 3. (a) The intrinsic viscosities [$|\chi|/f_a = 0, 0.04$ without (solid) and with (dashed) noise, respectively] and (b) normalized active viscosities, which follow Eq. (15) in the phase-locked regime, for the bead-spring triangles.

and/or rotation for appropriate values of α_{ij} [27]. In the absence of any external flow, and for $\alpha_{12} = \alpha_{13} = 0$ and $\alpha_{23} = \alpha \neq 0$, the swimmer performs translational motion.

In general, the nonlinear nature of Eq. (8) precludes analytical tractability. However, for $f_a \ll k$, the magnitude of swimmer deformation remains small (proportional to f_a/k), and an analytical perturbation analysis around the equilibrium shape of the triangular microswimmer becomes possible. As shown previously [27], in the absence of any external flow the stresslet associated with this triangular microswimmer vanishes over the course of one cycle of active force. Therefore, for $\mathbf{u}^\infty = 0$ it is a neutral swimmer and cannot be classified as puller or pusher [27]. However, we will see later that this result does not hold anymore in the presence of shear flow and the average stresslet takes a nonzero value (Sec. III A).

Under a linear shear flow, the contribution of the triangle to the suspension viscosity is given by the Kramers-Kirkwood formula [30]

$$[\eta] = -\frac{1}{v_b \dot{\gamma} \eta} \sum_i \langle y_i(t) f_i^x(t) \rangle, \tag{10}$$

where v_b is the swimmer volume, $y_i(t)$ is the y coordinate of the ith bead, and f_i^x is the x component of the total (active+passive) force acting on it. The resulting rheology is obtained numerically and shows the same qualitative features as in the case of the amoeboid model (Fig. 3). To unravel the mechanisms that govern the observed transitions (from positive to negative active viscosity as a function of shear rate) we will, in the following, analytically quantify the coupling of the active forces and applied flow.

III. ANALYTICAL CALCULATIONS

A. Triangle dynamics and phase-locking

For a passive vesicle or bead-spring triangle, one can describe the respective dynamics under shear flow in terms of the particle orientation φ_s (see Appendix B for details). Therefore, the time averaging in Eqs. (7) and (10) for the passive particles can also be achieved by an averaging over φ_s. On the other hand, activity affects shape and thus the swimmer orientation. The phase related to activity is $\varphi_a = \omega_a t$, whereas the phase related to shear flow driven shape change is $\varphi_s = \omega_s t$ where, due to symmetry (rear-front symmetry), the shape changes occur at a frequency twice the tumbling frequency ($\omega_s \simeq \dot{\gamma}$; as for the classical Jeffery orbit). This means that the shape configuration depends on both phases. For $\dot{\gamma} \ll \omega_a$ and $\dot{\gamma} \gg \omega_a$ (weak coupling), φ_s can

be considered independent of the activity and the time averaging in Eqs. (7) and (10) has to be performed over the larger period ($4\pi/\dot{\gamma}$ or $2\pi/\omega_a$). For $\dot{\gamma} \approx \omega_a$, however, there is a strong coupling between the swimmer orientation φ_s and its activity, so that φ_a becomes relevant as well. For weak deformation we have (which is an exact relation for a rigid object)

$$\frac{d\varphi_s}{dt} \approx \frac{1}{l^2}\left|\sum_{i=1}^{3} \mathbf{r}_i(\varphi_s, \varphi_a) \times \dot{\mathbf{r}}_i(\varphi_s, \varphi_a)\right|, \tag{11}$$

where $\mathbf{r}_i$ is the position vector of the ith bead. The evolution equation of a bead position is expressed as a proportionality between $\dot{\mathbf{r}}_i(\varphi_s, \varphi_a)$ and the total force acting on the bead. The active part contains obviously φ_a and the beads positions (via the spring force), which can be written as a function of φ_s to leading order in deformation. Together with definition (11) the time evolution of φ_s can be derived (see Appendix B).

If hydrodynamic interactions are ignored, along with the assumptions $f_a \ll k$ and $\dot{\gamma}, \omega_a \ll k\mu/l$, the phase equation assumes a simple analytical form, known as the Adler equation [31],

$$\frac{d\delta}{dt} \approx -(\dot{\gamma} - \omega_a) + A\dot{\gamma}\,\sin(\delta + \delta_0), \tag{12}$$

where $\delta = \varphi_s - \varphi_a$,

$$\cos\delta_0 = \frac{3 - 3\cos\alpha - 2\,\sin\alpha/\zeta}{\sqrt{2(1-\cos\alpha)(9 + 4/\zeta^2)}}, \tag{13}$$

and

$$A = 2\sqrt{2}\left(\frac{\sqrt{1-\cos\alpha}}{\sqrt{9 + 4/\zeta^2}}\right)\frac{f_a}{k} \tag{14}$$

depends on the magnitude of the triangle deformation (f_a/k) due to the active force (see Appendix B for a more general form of the Adler equation for the active triangle). In the above expressions, $\zeta = k\mu/\omega_a l$ is the ratio of the timescales associated with active force ($\sim 1/\omega_a$) and elastic deformation ($\sim l/k\mu$).

Equation (12) is a well-known equation in nonlinear systems and is used as a model for synchronization of oscillators [32,33]. It is apparent from Eq. (12) that for $-A \leqslant (\dot{\gamma}/\omega_a - 1) \leqslant A$ there is a "locking" of the two phases ($d\delta/dt = 0$) and we obtain $\dot{\gamma}_\mp = \omega_a(1 \mp A)$ as the boundaries of the "phase-locked" regime (see Supplemental Material movies in [34]). The phase-locking range $-A \leqslant (\dot{\gamma}/\omega_a - 1) \leqslant A$ evolves linearly with the active force (A is proportional to the active force). This behavior is also observed for the amoeboid swimmer [Fig. 2(b)].

The phase-locking phenomenon can be appreciated by analyzing the dependence of angular frequency of the shear flow driven triangle dynamics (ω_s) on the applied shear. By definition, the angular frequency ω_s is twice the tumbling frequency due to the symmetry of the shear flow. Figure 4(a) shows that ω_s increases with the shear rate monotonically, except in the phase-locked regime where the synchronization of shear and activity modes results in $\omega_s = \omega_a$. The phase-locking phenomenon also influences the "puller/pusher" nature of the swimmer as the swimmer stresslet changes its sign in the phase-locked regime, Fig. 4(b) (more details in Sec. IV). The effect of phase-locking is further reflected in the time dependence of the shear stress applied by the swimmer on fluid (Fig. 5). In the absence of activity under flow the particle has a cyclic motion with frequency ω_s (with the leading deformation mode behaving as $e^{i\omega_s t}$ + c.c.). The mode associated with activity is $e^{i\omega_a t}$ + c.c. Due to nonlinear coupling, this generates new modes having frequencies $\omega_s \pm \omega_a$. In the phase-locked regime ($\omega_s \approx \omega_a$) the system shows two frequencies: the basic one ω_a and $2\omega_a$ (Fig. 5, middle panels). Outside the phase-locked regime the system shows three disparate basic frequencies (generically, not rationally related to each other) ω_a and $\omega_s \pm \omega_a$, as seen in Fig. 5 (top and bottom panels).
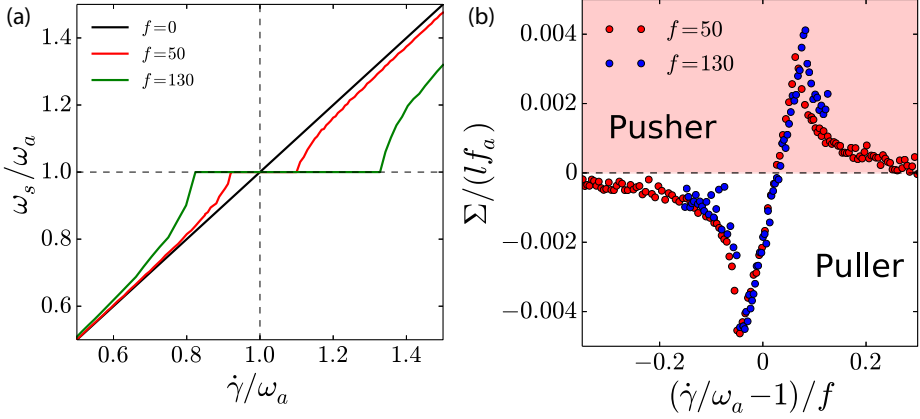
FIG. 4. Dependence of (a) ω_s, the angular frequency of the shear flow driven dynamics, and (b) the average stresslet Σ for the bead-spring swimmer, as a function of applied shear rate, $\dot{\gamma}$.

B. Effect of phase-locking on effective viscosity

In the phase-locked regime by using Eq. (10) we get

$$\frac{\Delta\eta}{[\eta]_p} \approx \frac{[3\zeta(\cos\alpha - \sin\alpha - 1) + 2(\cos\alpha + \sin\alpha - 1)]}{\sqrt{(9\zeta^2 + 4)(1 - \cos\alpha)}}\left(\frac{\omega_a}{\dot{\gamma}}\right)^2\left(\frac{\dot{\gamma}}{\dot{\gamma}_c} - 1\right), \qquad (15)$$

where

$$\dot{\gamma}_c = \omega_a\left[1 + 3\zeta^2\sqrt{\frac{2(1 - \cos\alpha)}{9\zeta^2 + 4}}\left(\frac{\cos\alpha + \sin\alpha - 1}{3\zeta(\cos\alpha - \sin\alpha - 1) + 2(\cos\alpha + \sin\alpha - 1)}\right)\left(\frac{f_a}{k}\right)\right]. \quad (16)$$

A first important result is that the active viscosity contribution changes sign at $\dot{\gamma} = \dot{\gamma}_c$. As we have seen before, this change of sign is related to a change of sign of the stresslet (pusher-puller transition; Fig. 4(b); see also next section). The value of this critical shear rate (due to the α dependence), $\dot{\gamma}_c$, can increase or decrease with f_a. It is remarkable that $\Delta\eta/[\eta]_p$ is independent of f_a in the phase-locked regime [Fig. 3(b)], which is also observed for the amoeboid swimmer [Fig. 2(b)]. The effect of active force amplitude f_a, however, does reflect in the maximum change in the viscosity,
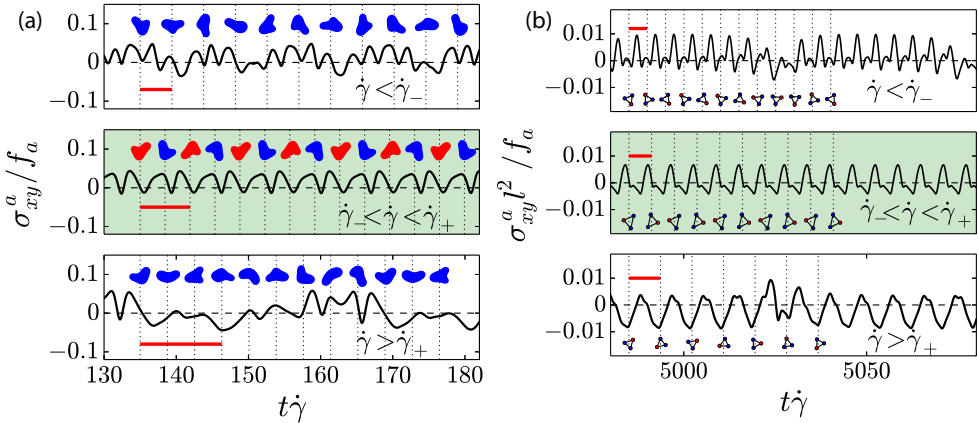

FIG. 5. Time dependence of the shear stress for (a) amoeboid and (b) bead-spring swimmers. Each panel also shows the evolution of swimmer conformations, showing a periodic character in the phase-locked regime (middle panels). The red bars designate the duration of the active force cycle.
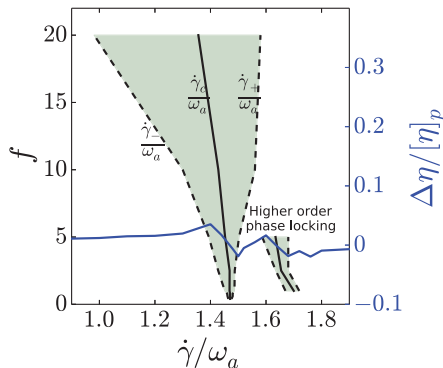
FIG. 6. Phase-locked regimes of the amoeboid swimmers for different f. $\Delta\eta/[\eta]_p$ for $f = 5.0$ is shown as a reference.

that is, $|\Delta\eta/[\eta]_p|_{\max}$, which is obtained by substituting $\dot{\gamma} = \dot{\gamma}_{\mp}$ in Eq. (15). Since $\dot{\gamma}_{\mp}$ scale linearly with f_a (at least for $f_a \ll k$), we have $|\Delta\eta/[\eta]_p|_{\max} \sim f_a$. It needs to be noted that this linear relation between maximum viscosity change and f_a holds for $f_a \ll k$. For large f_a the deformation of the triangle with linear springs may become so large that the perturbation analysis ceases to be valid.

Further, note that higher order phase-locking may also take place and Eq. (12) can be extended for $\delta_{mn} = m\varphi_s - n\varphi_a$ where $m \neq 0$ and $n \neq 0$ are arbitrary integers. The occurrence of higher order phase-locking suggests multiple values of critical shear rates $\dot{\gamma}_c$ where a transition between shear-thickening and shear-thinning behaviors can be observed (Fig. 6). A noteworthy point is that hydrodynamic interaction is not essential for the reported feature in Fig. 3(a), albeit necessary for the self-propulsion.

The phase-locking is found to be robust against several perturbations. For microscopic swimmers noise may have a significant effect on their behavior. In order to study the influence of noise on the swimmer behavior under shear flow and the phase-locking phenomenon we consider the noise to be of two origins. The first one is intrinsic: originating from activity. The intrinsic nature ensures that it does not contribute to the total force and torque. The second origin stems from fluctuations in the surrounding fluid. These fluctuations in fluid flow result in additional velocities to each bead of the triangular swimmer, which we assume to be uncorrelated over time as well as among the beads. We consider the combined effect of noise from these two sources in the form of random forces (proportional to the velocity fluctuations in the fluid) $\chi_i(t)$ on each bead such that they are uncorrelated, that is, $\chi_i(t)\chi_j(t') = |\chi|^2\delta_{ij}\delta(t - t')$ where $|\chi|$ is the noise amplitude. The noise from the fluid perturbations (external to the swimmer) results in a nonzero contribution to the total force and torque, resulting in translational and rotational diffusion of the swimmer. We performed numerical simulations of the bead-spring swimmer with noise under shear flow using the Euler-Maruyama method for the stochastic ordinary differential equations [35]. As shown in Fig. 3(a) the noise does not affect the qualitative features of the suspension viscosity as long as $|\chi| \ll f_a$. The consideration of noise reflects in the form of an additional diffusive term in the Adler equation [Eq. (B7)] resulting in the diffusion of the phase difference δ on a tilted washboard potential with occasional phase slips [33] as opposed to its deterministic behavior.

IV. MECHANISMS LEADING TO THE VISCOSITY BEHAVIOR

The microswimmers are usually categorized as puller or pusher depending on the far-field velocity field generated by the swimmer. The leading order contribution in the far-field velocity due to the swimmer can be written in terms of the first moment of the force distribution, that is, $\Sigma_{ij} = \sum_{i=1}^{3} \mathbf{f}_i \otimes \mathbf{r}_j$ for the bead-spring swimmer where $\mathbf{r}_i$ and $\mathbf{f}_i$ are the position and the total force on the ith bead. In the absence of any external flow (such as shear flow in this paper), the
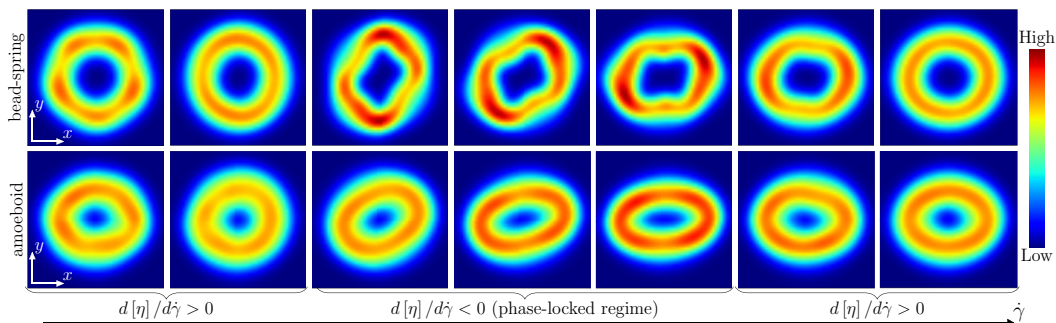
FIG. 7. Probability density of the presence of a bead (for triangle, upper panels) and swimmer membrane (for amoeboid, lower panels) under shear flow in the reference frame cotranslating with the swimmer center.

symmetric nature of the swimmer results in an average velocity field over one active force cycle to be proportional to the average stresslet $\Sigma_s = \Sigma_{xx} - \Sigma_{yy}$ where x is the direction of the swimmer propulsion. The puller and pusher nature of the swimmer is characterized by the sign of the stresslet Σ_s ($\Sigma_s < 0$ for puller and $\Sigma_s > 0$ for pusher). The bead-spring triangular swimmer with three identical beads is known to demonstrate a puller and pusher characteristic within an active force cycle, so that on average it acquires a neutral nature ($\Sigma_s = 0$) [27]. In the presence of a shear flow the triangle demonstrates tumbling and we can define the stresslet in the reference frame attached to the swimmer as $\Sigma = \Sigma_{x'x'} - \Sigma_{y'y'}$ where the swimmer propulsion direction x' is corotating with it. We calculated the average value (over sufficiently long time to capture the effects of interaction between shear and activity modes) of stresslet Σ of the bead-spring swimmer under different shear rates. Figure 4(b) shows the transition of the swimmer nature from pusher ($\Sigma < 0$) to puller ($\Sigma > 0$) at a shear rate close to the angular frequency of the active force. This transition between the two swimmer states coincides with the transition from $\Delta \eta > 0$ to $\Delta \eta < 0$. This demonstrates that for shape-deformation driven swimmers the puller-pusher nature is not an intrinsic property but depends on the external conditions, such as external flow (as shown here) or confinement [17].

In order to dig further into the origin of the viscosity change, we investigated the probability density of the microswimmer surface (or beads in the case of the bead-spring microswimmer) being at any location in the reference frame comoving with the swimmer center of mass. This density represents the average microswimmer shape in the steady state (Fig. 7). For low $\dot{\gamma}$ the average shape first has an increasing cross section against the flow (meaning shear thickening), then a decrease of cross section until alignment with the flow in phase-locked regime, then an increase of cross section with $\dot{\gamma}$. These behaviors are fully correlated with the finding presented in Figs. 2 and 3. In the phase-locked regime the swimmer takes only a certain sequence of shapes (see Supplemental Material movies [34]) and its average orientation gets aligned with the flow direction on increasing $\dot{\gamma}$ (Fig. 7). This alignment results in the shear-thinning behavior in the phase-locked regime. Outside the phase-locked regime, however, the swimmer attains many more shapes (see Supplemental Material movies [34]) and the average orientation distribution is relatively isotropic, resulting in shear-thickening behavior.

V. DISCUSSION

The phase-locking is very generic due to nonlinear coupling of two oscillators. Shear flow can lead to tumbling (which is the first autonomous oscillator). This is the case, for example, for *Chlamydomonas*, which undergoes (more or less complex) tumbling (see [8]). On the other hand, the activity is materialized by a periodic beating of flagella (the second oscillator). The flow affects the motion of flagella, which in turns affects the tumbling dynamics, resulting in an effective coupling between the two oscillators (the activity mode and the tumbling one). We thus expect phase-locking

to occur for various swimmers since tumbling and shape activity are quite common. Phase-locking (at least the first order) seems to be absent for shakers [Eq. (B7)]. It should be pointed out that the mechanism of viscosity modulation by the swimmer activity shown here is fundamentally different from the previously known mechanisms which rely primarily on the stochastic effects arising from the rotational diffusion or run-and-tumble nature [6,10,12,15] of the microswimmer. In general, however, the two mechanisms, deterministic (shape activity as reported here) and stochastic, can be visible under different applied shear rates for the same microswimmer. For shear rates significantly different from that of the angular frequency ω_a of the swimming strokes, we may expect the stochastic mechanism to prevail. In contrast, in the regime where the shear rate is close enough to ω_a the deterministic mechanism takes over. Equation (15) shows that in the phase-locked region (but for $\dot{\gamma} \neq \omega_a$) the active contribution to viscosity scales as $\Delta \eta / [\eta]_p \sim (\omega_a / \dot{\gamma})^2 \sim 1$. On the other hand, for fixed shapes (slender body) with noise it is of the order of $\Delta \eta / [\eta]_p \sim t_r / 15 t_s$ [15], where t_r and t_s are reorientation and swimming time (over swimmer size), respectively. For several swimmers [8,13,15] the latter leads to $\Delta \eta / [\eta] \sim 1$, meaning that shape activity contribution may be of the same order as that of noise. A systematic analysis will be needed before drawing conclusive answers about relative contributions of the two mechanisms.

Known experimental measurements of the active suspension viscosity have been performed for $\dot{\gamma} \ll \omega_a$ [8,13,14]. Explorations in the regime $\dot{\gamma} \approx \omega_a$ are needed to unravel the effect of shape deformation. For flagellar microswimmers such as *E. coli* and *C. reinhardtii*, $\omega_a \approx 100\pi$ s^{-1}. Thus high enough shear rates are required for the phase-locking. In contrast, amoeboid swimmers [3,4] are endowed with much longer stroke duration, approximately a few seconds, requiring much lower shear rates. Finally, it will be an interesting task for future research to study multiple swimmers in order to analyze the interplay between their mutual coupling (which may trigger their synchronization) and the effect of external flow.

ACKNOWLEDGMENTS

APPENDIX A: NUMERICAL SIMULATION OF AMOEBOID MICROSWIMMER USING BOUNDARY INTEGRAL METHOD

We consider a single swimmer in a linear shear flow

$$\mathbf{u}^\infty = \dot{\gamma} y \hat{\mathbf{e}}_x. \tag{A1}$$

Considering very small Reynolds number, the flow can be regarded as a Stokes flow and we can use the boundary integral method [22] to convert the Stokes equations into an integral form over the swimmer shape. The velocity at any point $\mathbf{r}$ in the domain can then be calculated by the boundary integral equation

$$\Lambda(\mathbf{r})\mathbf{u}(\mathbf{r}) = \mathbf{u}^\infty(\mathbf{r}) + \frac{1}{\eta} \oint \mathbf{F}(s') \cdot \mathcal{G}(\mathbf{X}(s'), \mathbf{r}) ds'$$

$$+ (1 - \lambda) \oint \mathbf{u}(\mathbf{X}(s')) \cdot \mathcal{T}(\mathbf{X}(s'), \mathbf{r}) \cdot \mathbf{n}(\mathbf{X}(s')) ds', \tag{A2}$$

where $\mathcal{G}$ and $\mathcal{T}$ are the single- and double-layer Green's functions, respectively, and the integrals are performed over the swimmer surface. The term Λ is defined as

$$\Lambda(\mathbf{r}) = \begin{cases} \lambda, & \text{if } \mathbf{r} \text{ is inside the swimmer} \\ (1+\lambda)/2, & \text{if } \mathbf{r} \text{ is on a swimmer surface} \\ 1, & \text{if } \mathbf{r} \text{ is outside of the swimmer.} \end{cases} \tag{A3}$$

Once the velocity on the membrane is known, the evolution of vesicle shape is obtained from a simple fixed time step Euler scheme

$$X_k(t + \Delta t) = X_k(t) + u_k(t)\Delta t, \tag{A4}$$

where $u_k(t)$ is obtained by taking Fourier transform of the velocity calculated from Eq. (A2) at time t. Ideally, fluid incompressibility and membrane impermeability should automatically ensure the swimmer volume to be a constant but a drift due to numerical scheme cannot be ruled out. To correct this drift, we inflate or deflate the swimmer through homogeneous normal deformation.

We performed several confirmatory simulations with refined meshes and time steps, sampling points, and Fourier harmonics to ensure the numerical accuracy of the scheme. This verification led us to compromise between efficiency and accuracy and characterize each swimmer surface by 63 Fourier harmonics. Further, we used 2048 sampling points to resolve the short-range hydrodynamics interactions. We calculated the swimmer surface velocity at 128 sampling points.

APPENDIX B: BEAD-SPRING MICROSWIMMER

1. Passive triangle in shear flow

We can obtain the passive counterpart of the active bead-spring microswimmer by setting $f_a = 0$. Once it is placed in shear flow $\dot{\gamma}$ it undergoes rotation and also oscillatory deformations. For $\dot{\gamma} \ll k\mu/l$ it is easy to see that the timescale of triangle rotation and deformation is $4\pi/\dot{\gamma}$. For small $\dot{\gamma}$ we can define the phase of the passive triangle φ_s as the angle made by one of the triangle beads with some prespecified direction in the triangle plane. Therefore, all the properties of the passive triangle under shear can be written in terms of φ_s. We can write the contribution of the passive triangle to total shear stress in the form of Kramers-Kirkwood stress [30] as

$$\sigma_{\text{KK}}^{xy} = \left\langle \sum_{i=1}^{3} f_i^x(\varphi_s) y_i(\varphi_s) \right\rangle, \tag{B1}$$

where averaging is performed over $\varphi_s \in [0, 2\pi]$, that is, all triangle configurations. For small triangle deformation, the force on any bead can be approximated as $f_i^{x,y}(\varphi_s) = \sum_{n=1}^{3} \sum_{j \neq i} [P_{ij}^{x,y} \sin(n\varphi_s) + Q_{ij}^{x,y} \cos(n\varphi_s)]$, where the $n\varphi_s$ dependence is due to the threefold symmetric shape of the triangle. Similarly, the small deformation assumption also gives $y_i(\varphi_s) = R_i \sin\varphi_s + S_i \cos\varphi_s$. The coefficients $P_{ij}^{x,y}$, $Q_{ij}^{x,y}$, R_i, and S_i are determined from the equations of motion of the beads [Eq. (8)]. Substituting the values of these coefficients in Eq. (B1) gives the effective viscosity of the passive bead-spring triangle suspension to be

$$\eta_p = \eta + \frac{\phi}{v_b} \frac{\sigma_{\text{KK}}^{xy}}{\dot{\gamma}} \approx \eta + \frac{\phi}{v_b} \frac{9l^2}{4\mu} \left(\frac{1}{c^2 + 9} \right), \tag{B2}$$

where v_b is the swimmer volume, ϕ is the swimmer volume fraction in the suspension, and $c = \dot{\gamma}l/k\mu$ is the capillary number. This demonstrates a shear-thinning behavior of the passive triangle under shear flow.

2. Active triangle in shear flow

a. No coupling between the shear flow driven dynamics and activity

For the active triangle in shear flow, if we do not consider any coupling between the shear flow and activity driven dynamics, the triangle undergoes tumbling at a constant rate (due to shear flow) and deformation (due to activity as well as flow). In the absence of the coupling, the two modes, activity and shear flow, are independent of each other and all dynamical variables can be written in terms of $\varphi_s = \dot{\gamma}t/2$ and $\varphi_a = \omega_a t$. Therefore, we can follow the same steps as for the passive triangle above. However, there are additional terms due to the triangle activity in the expressions for the force on the bead and with additional dependence on activity which gives $f_i^{x,y}(\varphi_s) = \sum_{j\neq i}\{[P_{ij}^a \sin(\omega_a t) + Q_{ij}^a \cos(\omega_a t)]\sin(\varphi_s) + [\tilde{P}_{ij}^a \sin(\omega_a t) + \tilde{Q}_{ij}^a \sin(\omega_a t)]\cos(\varphi_s)\}$ + passive force, where coefficients P_{ij}^a, Q_{ij}^a, $\tilde{P}_{ij}^a$, and $\tilde{Q}_{ij}^a$ can be obtained by solving Eq. (8) for an isolated active triangle without any external shear flow. We substitute these values in Eq. (B1) and take an average over one cycle of active force to obtain

$$
\eta_a \approx \eta_p - \frac{\phi}{v_b}\left(\frac{f_a}{k}\right)^2 \frac{l^2}{2\mu}
$$

$$
\times \left(\frac{54[\cos(\alpha-\beta)+\cos\alpha+\cos\beta+3] + 4\sqrt{3}(9c\zeta+c/\zeta)[\sin\beta-\sin\alpha+\sin(\alpha-\beta)]+729\zeta^2}{(9\zeta+1/\zeta)(9\zeta+4/\zeta)(9+c^2)}\right)
$$

(B3)

to be the effective suspension viscosity in the absence of coupling between activity and shear flow driven dynamics. It can be seen that for a purely translation microswimmer ($\beta = 0$), we get

$$
\eta_a \approx \eta_p - \frac{\phi}{v_b}\left(\frac{f_a}{k}\right)^2 \frac{l^2}{2\mu}\left(\frac{108(2+\cos\alpha)+729\zeta^2}{(9\zeta+1/\zeta)(9\zeta+4/\zeta)(9+c^2)}\right),
$$

(B4)

which has a monotonic dependence on $\dot{\gamma}$ contrary to the observation in Fig. 2. Therefore, the interaction between the two modes of triangle deformation cannot be ignored and the assumption of $\varphi_s \sim t$ breaks down.

b. With coupling between the shear flow driven dynamics and activity

In order to study the effect of coupling we first need to obtain the dependence of φ_s on t. Under the assumption of small deformation of the triangle, we can write

$$
\frac{d\varphi_s}{dt} \approx \frac{1}{l^2}\sum_{i=1}^{3}\left(x_i(\varphi_s,\varphi_a)\frac{dy_i}{dt}(\varphi_s,\varphi_a) - y_i(\varphi_s,\varphi_a)\frac{dx_i}{dt}(\varphi_s,\varphi_a)\right),
$$

(B5)

where (x_i, y_i) are the coordinates of the ith bead. In this condition we can take $x_i(\varphi_s(t),\varphi_a(t)) = R_i^x \sin\varphi_s(t) + S_i^x \cos\varphi_s(t) + R_i^{ax} \sin\varphi_a(t) + S_i^{ax} \cos\varphi_a(t)$ and $y_i(\varphi_s(t),\varphi_a(t)) = R_i^y \sin\varphi_s(t) + S_i^y \cos\varphi_s(t) + R_i^{ay} \sin\varphi_a(t) + S_i^{ay} \cos\varphi_a(t)$. Substituting these values in the following equation for the phase difference

$$
\frac{d\delta}{dt} = \frac{d\varphi_s}{dt} - \frac{d\varphi_a}{dt}
$$

(B6)

gives us the time dependence of the φ_s since the phase of the activity $\varphi_a = \omega_a t$ is already known. In a more general setup, we can also have the activity described not by explicit time dependence but triangle configuration. We do not consider those cases here. Assuming the change in the phase φ_s to be slower than the swimmer activity, we can use a method of averaging. After substituting the aforementioned expressions for x_i and y_i in Eq. (B5) and taking the average over one cycle of the

active force, we obtain the following Adler equation:

$$\frac{d\delta}{dt} \approx -(\dot{\gamma} - \omega_a) + \frac{f_a}{k}\frac{\dot{\gamma}}{9\zeta + 4/\zeta}(A_c \cos\delta + A_s \sin\delta) \tag{B7}$$

with

$$A_c = -2(2\cos\alpha - 3\zeta\sin\alpha) + 3\sqrt{3}\zeta(\cos\beta - 1) + 2(\cos\beta + 1) + \sin\beta(3\zeta + 2\sqrt{3}), \tag{B8}$$

$$A_s = -2(2\sin\alpha + 3\zeta\cos\alpha) + 2\sqrt{3}\zeta(\cos\beta - 1) + 3\zeta(\cos\beta + 1) + \sin\beta(2 - 3\sqrt{3}\zeta). \tag{B9}$$

This demonstrates that for different α and β (which correspond to the distribution of the active force on the amoeboid swimmer surface) the phase-locking is observed under shear flow. The corresponding window of the shear rates, however, is dependent on the nature of the active force distribution (α and β). It can be seen that for $\alpha = \beta = 0$ (no propulsion) we get $A_c = A_s = 0$, implying lack of phase-locking.

[1] Eric Lauga and Thomas R. Powers, The hydrodynamics of swimming microorganisms, Rep. Prog. Phys. **72**, 096601 (2009).

[2] J. Elgeti, R. G. Winkler, and G. Gompper, Physics of microswimmers—Single particle motion and collective behavior: A review, Rep. Prog. Phys. **78**, 056601 (2015).

[3] J. Throndsen, Flagellates of Norwegian coastal waters, Nytt. Magasin for Botanikk **16**, 161 (1969).

[4] N. P. Barry and M. S. Bretscher, Dictyostelium amoebae and neutrophils can swim, Proc. Natl. Acad. Sci. USA **107**, 11376 (2010).

[5] M. Bergert, A. Erzberger, R. A. Desai, I. M. Aspalter, A. C. Oates, G. Charras, G. Salbreux, and E. K. Paluch, Force transmission during adhesion-independent migration, Nat. Cell Biol. **17**, 524 (2015).

[6] D. Saintillan, The dilute rheology of swimming suspensions: A simple kinetic model, Exp. Mech. **50**, 1275 (2010).

[7] K. Drescher, R. E. Goldstein, N. Michel, M. Polin, and I. Tuval, Direct Measurement of the Flow Field Around Swimming Microorganisms, Phys. Rev. Lett. **105**, 168101 (2010).

[8] S. Rafai, L. Jibuti, and P. Peyla, Effective Viscosity of Microswimmer Suspensions, Phys. Rev. Lett. **104**, 098102 (2010).

[9] K. Drescher, J. Dunkel, L. H. Cisneros, S. Ganguly, and R. E. Goldstein, Fluid dynamics and noise in bacterial cell-cell and cell-surface scattering, Proc. Natl. Acad. Sci. USA **108**, 10940 (2011).

[10] Y. Hatwalne, S. Ramaswamy, M. Rao, and R. A. Simha, Rheology of Active-Particle Suspensions, Phys. Rev. Lett. **92**, 118101 (2004).

[11] D. Saintillan, Extensional rheology of active suspensions, Phys. Rev. E **81**, 056307 (2010).

[12] S. C. Takatori and J. F. Brady, Superfluid Behavior of Active Suspensions from Diffusive Stretching, Phys. Rev. Lett. **118**, 018003 (2017).

[13] J. Gachelin, G. Mino, H. Berthet, A. Lindner, A. Rousselet, and E. Clement, Non-Newtonian Viscosity of *Escherichia Coli* Suspensions, Phys. Rev. Lett. **110**, 268103 (2013).

[14] H. M. Lopez, J. Gachelin, C. Douarche, H. Auradou, and E. Clement, Turning Bacteria Suspensions Into Superfluids, Phys. Rev. Lett. **115**, 028301 (2015).

[15] D. Saintillan, Rheology of active fluids, Annu. Rev. Fluid Mech. **50**, 563 (2018).

[16] L. Jibuti, W. Zimmermann, S. Rafai, and P. Peyla, Effective viscosity of a suspension of flagellar-beating microswimmers: Three-dimensional modeling, Phys. Rev. E **96**, 052610 (2017).

[17] H. Wu, M. Thiébaud, W.-F. Hu, A. Farutin, S. Rafaï, M.-C. Lai, P. Peyla, and C. Misbah, Amoeboid motion in confined geometry, Phys. Rev. E **92**, 050701(R) (2015).

[18] H. Wu, A. Farutin, W. F. Hu, M. Thiebaud, S. Rafai, P. Peyla, M. C. Lai, and C. Misbah, Amoeboid swimming in a channel, Soft Matter **12**, 7470 (2016).

[19] E. M. Purcell, Life at low Reynolds number, Am. J. Phys. **45**, 3 (1977).

[20] A. Farutin, S. Rafai, D. K. Dysthe, A. Duperray, P. Peyla, and C. Misbah, Amoeboid Swimming: A Generic Self-Propulsion of Cells in Fluids by Means of Membrane Deformations, Phys. Rev. Lett. **111**, 228102 (2013).

[21] Q. Wang and H. G. Othmer, Computational analysis of amoeboid swimming at low Reynolds number, J. Math. Biol. **72**, 1893 (2016).

[22] C. Pozrikidis, *Boundary Integral and Singularity Methods for Linearized Viscous Flow*, 1st ed. (Cambridge University Press, Cambridge, UK, 1992).

[23] G. K. Batchelor, The stress system in a suspension of force-free particles, J. Fluid Mech. **41**, 545 (1970).

[24] John F. Brady, The Einstein viscosity correction in *n* dimensions, Int. J. Multiphase Flow **10**, 113 (1983).

[25] Vincent Doyeux, Stephane Priem, Levan Jibuti, Alexander Farutin, Mourad Ismail, and Philippe Peyla, Effective viscosity of two-dimensional suspensions: Confinement effects, Phys. Rev. Fluids **1**, 043301 (2016).

[26] J. Fouchard, C. Bimbard, N. Bufi, P. Durand-Smet, A. Proag, A. Richert, O. Cardoso, and A. Asnacios, Three-dimensional cell body shape dictates the onset of traction force generation and growth of focal adhesions, Proc. Natl. Acad. Sci. USA **111**, 13075 (2014).

[27] M. S. Rizvi, A. Farutin, and C. Misbah, Three-bead steering microswimmers, Phys. Rev. E **97**, 023102 (2018).

[28] Benjamin M. Friedrich and Frank Julicher, Flagellar Synchronization Independent of Hydrodynamic Interactions, Phys. Rev. Lett. **109**, 138102 (2012).

[29] Kyriacos C. Leptos, Kirsty Y. Wan, Marco Polin, Idan Tuval, Adriana I. Pesci, and Raymond E. Goldstein, Antiphase Synchronization in a Flagellar-Dominance Mutant of *Chlamydomonas*, Phys. Rev. Lett. **111**, 158101 (2013).

[30] M. Doi and S. F. Edwards, *The Theory of Polymer Dynamics* (Oxford University Press, New York, 1998).

[31] R. Adler, A study of locking phenomena in oscillators, Proc. IRE **34**, 351 (1946).

[32] Yoshiki Kuramoto, Self-entrainment of a population of coupled non-linear oscillators, in *International Symposium on Mathematical Problems in Theoretical Physics*, edited by Huzihiro Araki (Springer, Berlin, Heidelberg, 1975), pp. 420–422.

[33] A. Pikovsky, M. Rosenblum, and J. Kurths, *Synchronization, A Universal Concept in Nonlinear Sciences*, 1st ed. (Cambridge University Press, Cambridge, UK, 2001).

[34] See Supplemental Material at http://link.aps.org/supplemental/10.1103/PhysRevFluids.4.103302 for movies showing the dynamics of amoeboid and bead-spring microswimmers for three shear rates ($\dot{\gamma} < \dot{\gamma}_-$, $\dot{\gamma}_- < \dot{\gamma} < \dot{\gamma}_+$, and $\dot{\gamma} > \dot{\gamma}_+$) in the reference frame comoving with the swimmer center of mass.

[35] Peter E. Kloeden and Eckhard Platen, *Numerical Solution of Stochastic Differential Equations* (Springer Science and Business Media, Berlin, 1992).